Digital Object Identifier 10.23919/EPE23ECCEEurope58414.2023.10264424

2023 25th European Conference on Power Electronics and Applications (EPE'23 ECCE Europe)

Losses Analysis of MMC in Medium Frequency Medium Voltage DAB Converter for Charging Station

Sattar Bazyar
Jun-Hyung Jung
Rui Li
Hamzeh Beiranvand
Marco Liserre

Suggested Citation

S. Bazyar, J. -H. Jung, R. Li, H. Beiranvand and M. Liserre, "Losses Analysis of MMC in Medium Frequency Medium Voltage DAB Converter for Charging Station," 2023 25th European Conference on Power Electronics and Applications (EPE'23 ECCE Europe), Aalborg, Denmark, 2023, pp. 1-9

Losses Analysis of MMC in Medium Frequency Medium Voltage DAB Converter for Charging Station

Sattar Bazyar[1], Jun-Hyung Jung[1], Rui Li[1], Hamzeh Beiranvand[1], Marco Liserre[1]
1. Chair of Power Electronics, Kiel University
Kaiserstraße 2, 24143 Kiel
Kiel, Germany
Tel.: +49 431 880-6100
E-Mail: {sab,jj,ruil,hab,ml}@tf.uni-kiel.de
URL: http://www.pe.tf.uni-kiel.de

Acknowledgment

Funded by the Deutsche Forschungsgemeinschaft (DFG, German Research Foundation)- project number (492987385).

Index Terms—Dual active bridge (DAB) converter, Medium frequency, Medium voltage, Modular multilevel converter (MMC), Power losses.

Abstract—Medium voltage (MV) modular multilevel converter (MMC) is an attractive candidate for multi MW fast charging station (FCS) to transfer high power with high efficiency, and a medium-frequency (MF) isolated dual active-bridge (DAB) DC/DC converter is needed to step down the voltage in this application. In this regard, MMC-based isolated DAB DC/DC converter is a good candidate to be used in FCS. In MMC-based isolated DAB DC/DC converter, Quasi-two-level (Q2L) waveform is the preferred waveform for the AC side voltage of MMC due to low dv/dt and small capacitor of submodules. The analysis on power losses of MMC in this application and with this specific AC voltage waveform is an important issue for a cellular high-efficiency design that requires more investigation. This paper provides an analysis to estimate switching and conduction losses of MMC used to produce a quasi-two-level waveform which can be used among the others also in DAB applications. Finally, the effectiveness of the losses analysis is verified by simulation results, and the experimental results are used to investigate the behavior of MMC in this application.

I. Introduction

The electric vehicle (EV) market has seen rapid growth in recent years, driven by policy encouragement to cope with the climate change crisis. In response to the high number of EVs being produced, many studies have been carried out on high-power fast charging stations (FCSs) [1], [2]. Fast charging of many EVs requires large-scale and high-power chargers. Since an on-board charger is designed with low-power converters due to the restriction of weight and space, it is hard to expect fast enough charging [3].

As another charging structure, conventional off-board chargers are composed of a low-frequency transformer, AC/DC converter and DC/DC converter. However, the efficiency of the charger is not high because this system is connected to a low-voltage (LV) AC grid which causes high losses with high current and it has many conversion stages [4]. To overcome this shortcoming, a charging station based on medium voltage DC (MVDC) grids is emerging. A modular multilevel converter (MMC) is an essential system enabling MVDC utilization because this converter is structured with serial-connected submodules (SMs) [5].

The MMC can be utilized as a primary converter of the dual-active-bridge (DAB) converter to connect FCS to the MVDC grid [6]. In conventional DAB converters, a rectangular waveform with a medium or high frequency is applied across a primary winding of the medium-frequency (MF) transformer to maximize power transfer efficiency instead of using the sinusoidal waveform with a low frequency. In the MMC-based DAB converter connected to MVDC grids, however, a quasi-two-level (Q2L) waveform is adapted rather than the rectangular waveform to avoid the galvanic isolation breakdown due to high dv/dt [7]–[9].

An important issue in MF MMC-based DAB converter is the analysis of losses, which is required to optimize the performance of the system and design the cooling system [10]. Since many SMs are employed in MMC, it is complex to calculate its power losses. In [10], the power losses are obtained by simulation of the system in MATLAB/Simulink. However, it is not effective when a large number of SMs are used in the structure of MMC. The average value model of MMC is obtained and utilized to calculate the power losses in [11]. However, this method has considered some simplified assumptions, such as the same power losses for all SMs, using average arm current and an approximated SM selector switching number function.

Although much research has been done to obtain the power losses, there is a lack of literature on power loss analysis based on instantaneous current in MMC-based DAB converter. In this regard, this paper analyzes the instantaneous AC and DC current based on the model of the converter. The arm current of MMC is derived based on the instantaneous waveform of AC current and DC current. Finally, these waveforms are employed to calculate the power losses of MMC. These losses include switching and conduction losses of semiconductors in SM, such as IGBTs and Diodes. These two losses are calculated separately and compared with the simulation results for both switches and diodes.

II. MMC-BASED DAB CONVERTER

The structure of the MMC-based DAB converter is shown in Fig. 1. Two-legs MMC, which has good scalability in terms of the DC voltage, are used as a primary side converter that is connected to the MVDC grid. The AC side of the MMC is connected to a medium-frequency transformer (MFT). On the secondary side, a H-bridge converter is placed, and it is operated with shifting a phase angle of PWM signals to transfer power to low-voltage output, which can be used for FCSs.

In conventional DAB converters, two-level rectangular voltage waveform with medium frequency is preferred to maximize the power transfer. However, in the case of DC/DC converters using MVDC, high dv/dt of the voltage output by the MMC causes a problem with galvanic isolation breakdown. For this reason, a Q2L waveform shown in Fig. 2 is suitable for MMC-based DAB converters. When the voltage waveform is rising and falling, a low dv/dt characteristic can be achieved owing to the staircase-shaped voltage change. The number of SMs in each

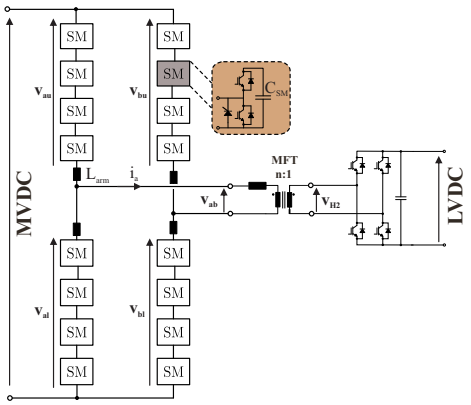

Fig. 1: MMC-based DAB converter for FCS

arm (N) of MMC determines the number of voltage changes, and the amount of voltage changes in each step at the AC side of MMC is equal to two times the corresponding SM capacitor voltage (V_C).

There are two representative modulation techniques to create the Q2L waveform, nearest-level modulation (NLM) [12] and phase-shift modulation (PSM) [13]. NLM is a modulation technique that determines the number of SMs to insert into the arm of the MMC based on the magnitude of the voltage waveform. That's why it is a popular modulation for high-level MMCs used for high-voltage DC transmission applications. In the case of the MMC-based DAB converter, the number of SMs to be inserted is determined according to the magnitude of an input trapezoidal waveform, as shown in Fig. 3(a), and transition time (T_{tr}) between voltage changes is related to the slope of the trapezoidal waveform. Regarding the SM DC capacitor voltage balancing, it is required to apply a sorting algorithm-based balancing method, similar to the case of general MMCs [12]. It is worth noting that the NLM technique can cause more losses depending on how it changes the SM insertion states. In addition, this modulation wouldn't be suitable for generating high-frequency waveform, compared to carrier-based modulations, due to computational burden.

The second popular modulation technique for generating the Q2L waveform is PSM, based on carrier-based PWM. As shown in Fig. 3(b), each SM can be operated by PWM signals with a 50% duty cycle, and the signals for each SM are shifted as much as the transition time between voltage steps in the Q2L waveform since the phase of the carriers applied to each SM is shifted. Even though it is easy to generate gate signals using the carriers, it requires rotating the gate signals, which is complicated to implement in

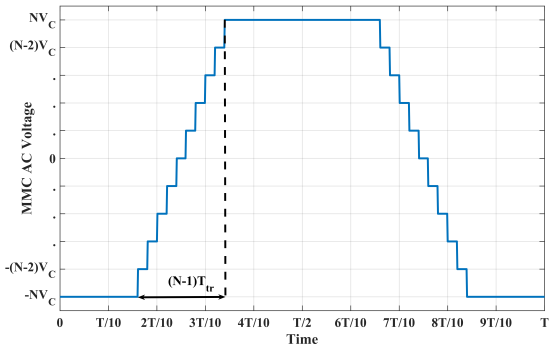

Fig. 2: Q2L waveform for MMC-based DAB converters

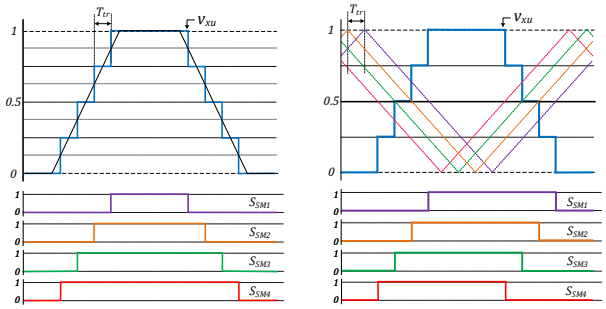

(a) (b)

Fig. 3: Modulation techniques for the Q2L waveform: (a) NLM, (b) PSM

practice, to balance SM DC capacitor voltage.

In this paper, the analysis of current and semiconductor losses is carried out, supposing the PSM technique is applied to MMC. Also, to calculate switching and conduction losses of each switch and diode, Fig. 4 is used, which shows the current path in different SM state and current directions.

III. Loss Analysis of MMC in DAB Converter

In this part, a procedure to calculate conduction and switching losses of MMC will be discussed.

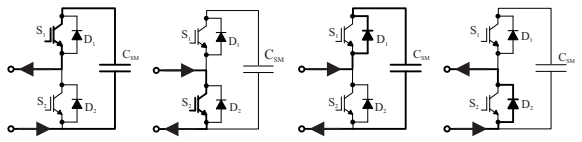

(a) (b) (c) (d)

Fig. 4: Different modes of HBSM: (a) S_1: on, S_2: off, $i_{arm} < 0$, (b) S_1: off, S_2: on, $i_{arm} > 0$, (c) S_1: on, S_2: off, $i_{arm} > 0$, (d) S_1: off, S_2: on, $i_{arm} < 0$

Since arm current and voltage of MMC is required to calculate switching and conduction losses, basic equations to obtain arm voltage and current of MMC will be explained in this part. In the single-phase MMC shown in Fig. 1, upper and lower arm voltages are obtained as follows.

$$v_{xu} = \frac{v_{DC}}{2} - v_{ab} \tag{1}$$

$$v_{xl} = \frac{v_{DC}}{2} + v_{ab} \tag{2}$$

where $x \in \{a, b\}$ shows the related leg, and v_{DC} and v_{ab} are the DC side voltage and AC side voltage of MMC, respectively. Also, v_{xu} and v_{xl} denote the upper and lower arm voltage of each leg. Also, the arm current of MMC can be written as follows.

$$i_{xu} = \frac{i_{DC}}{2} - \frac{i_x}{2} \tag{3}$$

$$i_{xl} = \frac{i_{DC}}{2} + \frac{i_x}{2} \tag{4}$$

where i_{xu} and i_{xl} are the upper and lower arm currents, respectively. Moreover, i_{DC} and i_x represent the DC side and AC side current of MMC, respectively.

Based on these equations, AC side and DC side current and voltage of MMC is necessary to calculate arm currents and voltages. To obtain DC and AC currents and voltages, the equivalent circuit of MMC and other parts of the system should be derived. Therefore, in this section, the equivalent circuit of the system is acquired at first, and then, the equations to calculate DC and AC side currents are extracted based on this circuit. After that, the arm voltages and currents are determined based on (1) to (4). Finally, the conduction and switching losses are calculated by using the current and voltage waveform.

A. Equivalent Circuit of MMC-based DAB Converter

Since the structure of the MMC-based DAB converter is very similar to the structure of the conventional DAB converter, the DAB model is used in this part to obtain the equivalent circuit of the system [14]. The equivalent circuit of the conventional DAB is shown in Fig. 5 (a). As it can be seen, in this circuit, two voltage sources are usually connected to each other through an inductor. Each voltage source represents the AC side voltage of each H-bridge converter, which is a rectangular waveform, and an inductor is used to model the equivalent inductance between two sources, which is usually the leakage inductor of the transformer (L_t).

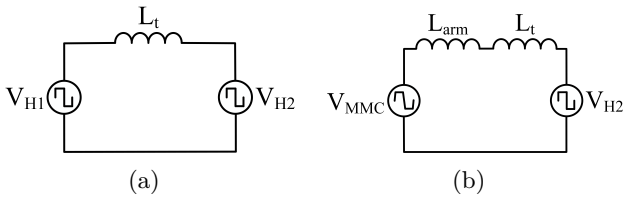

Fig. 5: Model of DAB system: (a) Conventional DAB, (b) MMC-based DAB

In the MMC-based DAB converter, the H-bridge converter at the primary side of the transformer is replaced by a single-phase MMC. Therefore, the equivalent circuit should be modified by considering the MMC model. In this case, it is assumed that MMC generates a Q2L waveform at the AC side, and the capacitor voltage is constant, but the arm inductance (L_{arm}) is considered in the model of the MMC, as it is shown in Fig. 5(b). Based on the average value model of MMC, since MMC includes two legs (four arms), and half of the AC side current is passed through each arm, the equivalent inductance of MMC is equal to the arm inductance [15].

As a result, MMC is modeled as a voltage source with a series inductor. Thus, the model of MMC-based DAB converter is the same as conventional DAB, but the generated voltage of MMC and the equivalent inductance is different. In conventional DAB, the H-bridge converter generates a rectangular waveform, but in this case, MMC creates a Q2L waveform. Also, in the conventional DAB, the equivalent inductance between two voltage sources is only leakage inductance of transformer, but in the MMC-based DAB converter, the equivalent inductance includes the arm inductance and the leakage inductance of transformer.

B. Arm Current Calculation

The arm current is necessary to calculate power losses of MMC, and it can be derived by using (3) and (4). Based on these equations, the AC and DC side current are required to determine the arm current. The DC side current (i_{DC}) can be be easily obtained according to the input power (p_{in}) and the input voltage (v_{in}) as follows.

$$i_{DC} = \frac{p_{in}}{v_{in}} \tag{5}$$

Regarding the AC side current, the equivalent model shown in Fig. 5 (b). is used. To use this model, two AC side voltages are needed. For simplicity, AC side voltage of MMC during transition time is approximated by a ramp waveform. In addition, the AC side voltage of H-bridge converter at the secondary side can be easily assumed as a square waveform. As a result, the AC side voltage of MMC and H-bridge converter can be defined as follows:

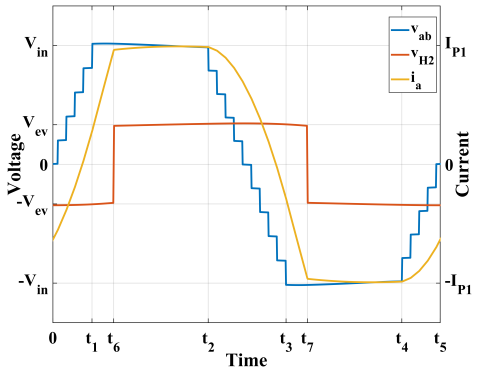

Fig. 6: Key waveforms of MMC-based DAB converter when $t_6 > t_1$

$$V_{ab} = \begin{cases} K\,t, & 0 \le t < t_1 \\ V_{DC}, & t_1 \le t < t_2 \\ V_{DC} - K(t - t_2), & t_2 \le t < t_3 \\ -V_{DC}, & t_3 \le t < t_4 \\ -V_{DC} + K(t - t_4), & t_4 \le t < t_5 \end{cases} \tag{6}$$

$$V_{H2} = \begin{cases} -V_{ev}, & 0 \le t < t_6 \\ V_{ev}, & t_6 \le t < t_7 \\ -V_{ev}, & t_7 \le t < t_5 \end{cases} \tag{7}$$

where $t_1 = (N-1)T_{tr}$, $K = \frac{V_{in}}{t_1}$ is the slope of ramp waveform, t represents time, and V_{ev} describes the DC side voltage of H-bridge converter at the secondary side of transformer. Moreover, t_6 determined the phase difference between AC voltage generated by MMC and AC side voltage of H-bridge converter.

Based on the equivalent model of the system, AC side current can be determined as follows.

$$i_a = \frac{1}{L_{eq}} \int_0^t (v_{ab}(t) - v_{H2}(t))\, \mathrm{d}t \tag{8}$$

According to the value of t_6 and t_1, two states are discussed. In the first one, which is shown in Fig. 6, t_6 is greater than t_1, and the AC side current is calculated as follows.

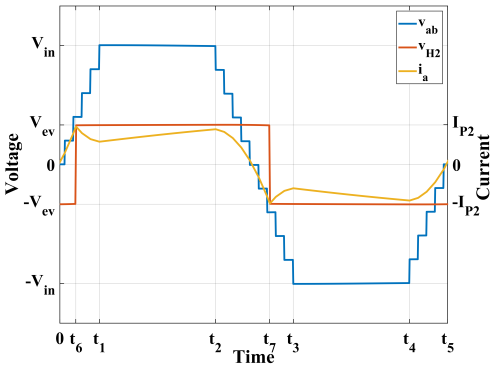

Fig. 7: Key waveforms of MMC-based DAB converter when $t_6 < t_1$

$$i_a = \begin{cases} i_a^0 + \frac{1}{2}k \times t^2 + nV_{ev}t, & 0 \le t < t_1 \\ i_a^{t_1} + V_{DC} \times t + nV_{ev}t, & t_1 \le t < t_6 \\ i_a^{t_6} + V_{DC} \times t - nV_{ev}t, & t_6 \le t < t_2 \\ i_a^{t_2} + V_{DC}t - \frac{1}{2}Kt^2 + Kt_2t - nV_{ev}t, & t_2 \le t < t_3 \\ i_a^{t_3} - V_{DC}t - nV_{ev}t, & t_3 \le t < t_7 \\ i_a^{t_7} - V_{DC}t + nV_{ev}t, & t_7 \le t < t_4 \\ i_a^{t_4} - V_{DC}t + \frac{1}{2}Kt^2 - Kt_4t + nV_{ev}t, & t_4 \le t < t_5 \end{cases} \quad (9)$$

where i_a^t describes the AC side current of MMC at time t. For instance, i_a^0 is the the AC side current of MMC at time 0, and it can be calculated by considering that $i_a^0 = -i_a^{\frac{T}{2}}$. Moreover, $t_5 = T$ is the operating period of the MMC.

In the second state depicted in Fig. 7, t_6 is less than t_1, and the AC side current can be obtained as follows.

$$i_a = \begin{cases} i_a^0 + \frac{1}{2}k \times t^2 + nV_{ev}t, & 0 \le t < t_6 \\ i_a^{t_6} + \frac{1}{2}k \times t^2 - nV_{ev}t, & t_6 \le t < t_1 \\ i_a^{t_1} + V_{DC} \times t - nV_{ev}t, & t_1 \le t < t_2 \\ i_a^{t_2} + V_{DC}t - \frac{1}{2}Kt^2 + Kt_2t - nV_{ev}t, & t_2 \le t < t_7 \\ i_a^{t_7} + V_{DC}t - \frac{1}{2}Kt^2 + Kt_2t + nV_{ev}t, & t_7 \le t < t_3 \\ i_at_3 - V_{DC}t + nV_{ev}t, & t_3 \le t < t_4 \\ i_at_4 - V_{DC}t + \frac{1}{2}Kt^2 - Kt_4t + nV_{ev}t, & t_4 \le t < t_5 \end{cases} \quad (10)$$

Based on the AC side and DC side current, the arm current is determined, and based on this arm current and switching commands, it is possible to calculate

TABLE I: The operating pattern of each SM

SM voltage	Arm current	S_1	D_1	S_2	D_2
+	+	-	✓	-	
+	-	✓	-	-	
0	+	-	-	✓	-
0	-	-	-	-	✓

different parameters of the MMC. For instance, the SM capacitance can be derived as follows.

$$C_{SM} = \frac{1}{\Delta V}\int_0^T i_{cap}(t)\,\mathrm{d}t \quad (11)$$

where i_{cap} is the instantaneous capacitor current, and ΔV is the desired capacitor voltage ripple, which is usually set between 5% to 20% of the nominal capacitor voltage. The capacitor current is obtained according to the arm current and switching commands. It means when switch S_1 or D_1 conducts the arm current, the capacitor current is equal to the arm current. But, when the arm current is passed through switch S_2 or D_2, the capacitor current is zero.

C. Determine Switching and Conduction Losses

Based on the analysis provided in subsection B, the arm current is obtained, and the arm voltage can be easily derived by substitution (6) into (1) and (2). Then Table.1 is used to realize which switch or diode is responsible to pass the current. For instance, when SM generates positive voltage at its AC terminal, and arm current is positive, the current is passed through diode D_1. Therefore, based on the arm current, arm voltage, and Table. 1, it is possible to calculate the current and voltage of each switch and diode, and based on that, the switching and conduction losses of each switch and diode are estimated. The conduction losses can be calculated as follows.

$$P_{cond,IGBT} = \frac{1}{T}\int_0^T v_{ce}(t) \times i_c(t)\,\mathrm{d}t \quad (12)$$

$$P_{cond,Diode} = \frac{1}{T}\int_0^T v_f(t) \times i_f(t)\,\mathrm{d}t \quad (13)$$

where $v_{ce}(t)$ and $v_f(t)$ are the on-state collector-emitter voltage of IGBT and on-state voltage of diode, respectively. In addition, $i_C(t)$ and $i_f(t)$ represent the collector current and forward current of diode during conduction, respectively. These parameters can be extracted based on the characteristics of diode and IGBT in datasheet.

The switching losses in IGBTs consist of two parts: turn-on losses and turn-off losses. To obtain these

losses, the Turn-on energy ($E_{on,IGBT}$) and turn-off energy ($E_{off,IGBT}$) of IGBT are required, and they are obtained as follows.

$$E_{on,IGBT} = E_{on,IGBT,n} \times \frac{I_c}{I_{c,n}} \times \frac{V_{ce}}{V_{ce,n}} \quad (14)$$

$$E_{off,IGBT} = E_{off,IGBT,n} \times \frac{I_c}{I_{c,n}} \times \frac{V_{ce}}{V_{ce,n}} \quad (15)$$

where $E_{on,n}$ and $E_{off,n}$ are the turn-on and turn-off energy losses at the nominal condition of IGBT, and I_c, n and $V_{ce,n}$ represent the nominal current and voltage of IGBT, respectively. In addition, I_c and V_{ce} describes the rms current and voltage of IGBT, respectively.

Then, based on turn-on and turn-off energy losses, total switching losses ($P_{SW,IGBT}$) are determined as follows.

$$P_{SW,IGBT} = \frac{1}{T}(\sum_{i=1}^{N_s} E_{on,IGBT} + \sum_{i=1}^{N_s} E_{off,IGBT}) \quad (16)$$

where N_s refers to the number of times that switch turns on or off in one period.

For diodes, turn-on losses are negligible, and only turn-off losses (or reverse recovery losses) are taken into account. To calculate turn-off losses, the turn-off energy should be obtained, and they are determined as follows.

$$P_{off,Diode} = E_{off,Diode,n} \times \frac{I_f}{I_{f,n}} \times \frac{V_D}{V_{D,n}} \times f \quad (17)$$

where $E_{off,Diode,n}$ is the nominal turn off energy losses of diode, $I_{f,nom}$ and $V_{D,nom}$ describes the nominal current and voltage of diode, respectively, and I_f and V_D represent the rms current and rms voltage of diode, respectively.

It is worth mentioning that in this paper, PSM is employed, and carriers are rotated at different periods to keep capacitor voltage and SM losses balanced. So, since the SM losses are equal, the total losses of each component at one arm are obtained based on the current and voltage waveforms, and it is divided by the number of SMs at each arm to calculate the losses of each component at one SM.

IV. Simulation and Experimental Results

To validate the provided analysis in this paper, an MMC-based DAB converter is simulated in MATLAB/Simulink and PLECS. The parameters of this system are described in Table 2. In this table, C_{SM} expresses the SM capacitance, and n is transformer turn ratio, respectively. Two scenarios are considered to investigate the accuracy of analysis to obtain power losses of MMC. In these two scenarios, it is assumed that the output voltage is 500 V, but different powers are transferred to the output load. In the first scenario, t_1 is greater than t_6, and in the second one t_1 is lower than t_6. These two scenarios are discussed in below.

TABLE II: Simulation Parameters

Parameters	V_{in}	V_{ev}	C_{SM}	L_{arm}
Value	10 kV	500 V	50 uF	2 mH
Parameters	T	T_{tr}	n	N
Value	1 ms	25 us	20	10

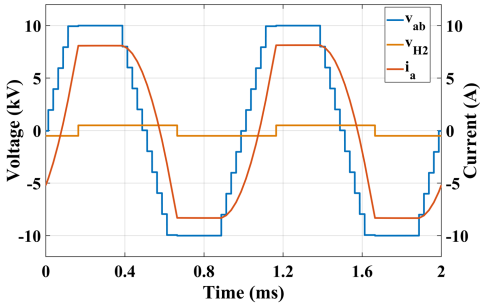

Fig. 8: AC voltage and current of MMC, and AC voltage of H-bridge when $t_6 > t_1$

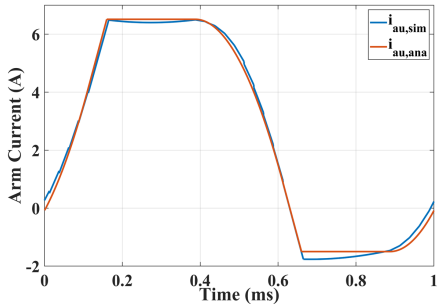

Fig. 9: upper arm current when $t_6 > t_1$

A. Losses Analysis when $t_1 > t_6$

In this scenario, the output power of the system is 50 kW. Fig. 8 shows the simulation results for this scenario, and it includes AC side voltage of MMC, AC side voltage of H-bridge converter, and AC side current of MMC. Based on the simulation results and provided analysis, the arm current is obtained, and they are compared in Fig. 9. As is seen, these two waveforms are very similar.

According to the provided analysis, arm voltage (approximated arm voltage (blue waveform) and exact arm voltage (purple waveform)) and current are shown in Fig. 10. Then, based on this figure and Table. 1,

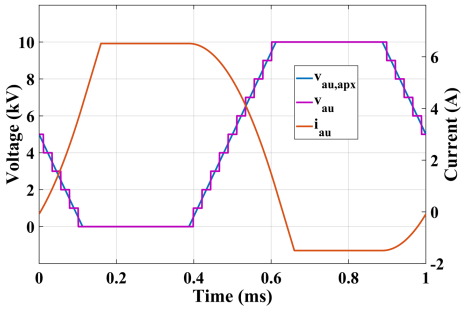

Fig. 10: upper arm current and voltage when $t_6 > t_1$

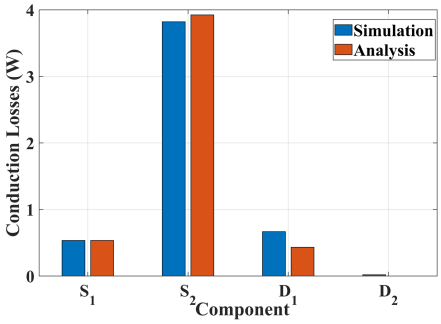

Fig. 11: Conduction losses of components when $t_6 > t_1$

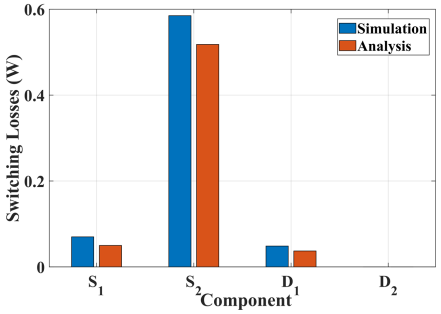

Fig. 12: Switching losses of components when $t_6 > t_1$

the current and voltage of each component can be derived, and then, conduction and switching losses can be determined by using (13) to (20). Fig. 11 and Fig. 12 provides a comparison between simulation and analysis results in the aspects of the switching and conduction losses, respectively. As is seen ,the switching and conduction losses derived by the analysis are very close to the losses obtained by simulation. The total losses in simulation is 5.74 W for each SM, while it is 5.49 W in the analysis, and So, it verifies the effectiveness of the analysis.

B. Losses Analysis when $t_1 < t_6$

In this scenario, it is assumed that $t_1 < t_6$, and the output power is 30 kW. The simulation results,

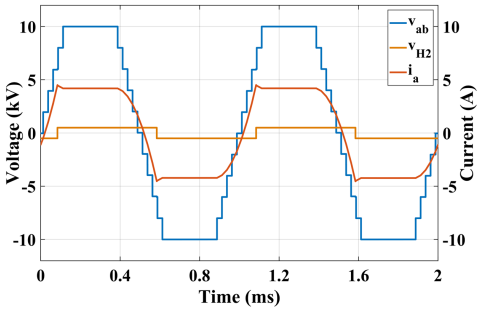

Fig. 13: AC voltage and current of MMC, and AC voltage of H-bridge when $t_6 < t_1$

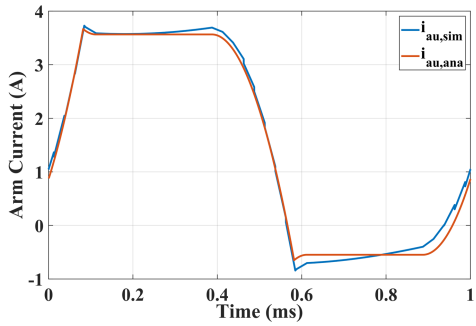

Fig. 14: upper arm current when $t_6 < t_1$

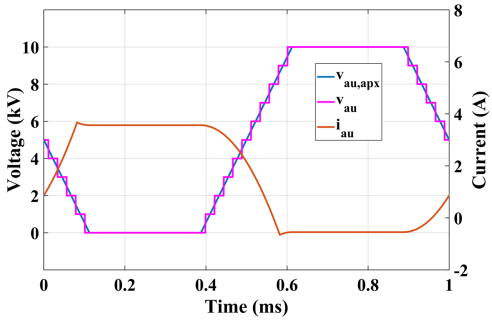

Fig. 15: upper arm current and voltage when $t_6 < t_1$

including AC side voltage of MMC, AC side voltage of H-bridge converter, and AC current of MMC, are shown in Fig.13. Like the first scenario, as seen in this figure, the phase difference between voltage generated by MMC and H-bridge converter is lower than the first scenario. The similar strategy to the first scenario is considered to calculate the arm current in this part. The only difference is using (10) instead of (9) to obtain the AC side current. Fig. 14 depicts the arm current that is obtained by simulation and analysis. In this case, the current waveform based on the analysis is very close to the simulation results.

Fig.15 depicts the upper arm current and arm voltage of MMC derived by the analysis. Based on this

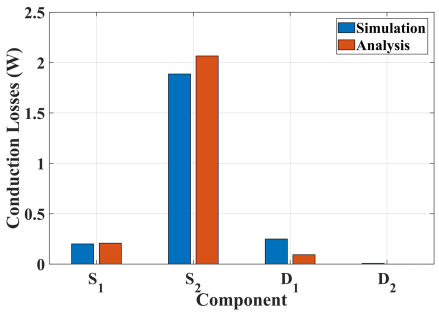

Fig. 16: Conduction losses of components when $t_6 < t_1$

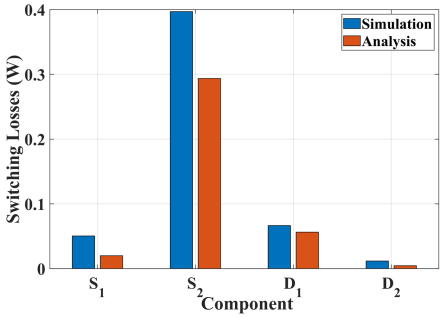

Fig. 17: Switching losses of components when $t_6 < t_1$

TABLE III: Parameters of experimental setup

Parameters	V_{in}	C_{SM}	L_{arm}	n
Value	100 V	56 uF	100 uH	1
Parameters	f	T_{tr}	L_{add}	N
Value	5 kHz	5 us	310 uH	4

current and voltage waveforms, the losses of MMC are calculated, and their results are compared with simulation results in Fig. 16 and Fig. 17. These results show that the total losses of MMC is 2.87 W in simulation, while it is 2.74 W in the analysis. As a result, the accuracy of the analysis to calculate losses is about 95%, which shows high accuracy of the analysis in this power rating.

The laboratory prototype related to a single-phase MMC with two legs and four SMs in each arm are shown in Fig. 18. The AC side of MMC is connected to an isolation transformer, and the secondary side of the transformer is connected to an H-bridge with an additional inductor (L_{add}). Finally, the DC side voltage of H-bridge is connected to a resistor as the load. The parameters of this setup are described in Table. 3. Fig. 19(a) depicts the AC side voltage and current of MMC, and also AC side voltage of H-bridge. As is seen, MMC generates a Q2L waveform at its AC side, and the AC side voltage of H-bridge is a two-level waveform. The AC side current of MMC is also

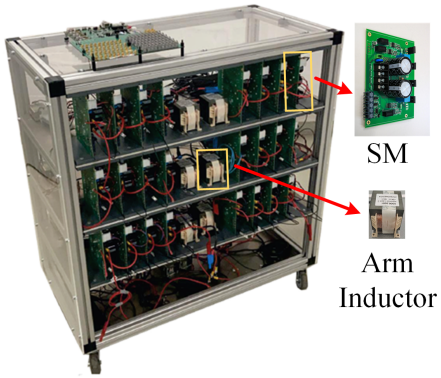

Fig. 18: Laboratory prototype

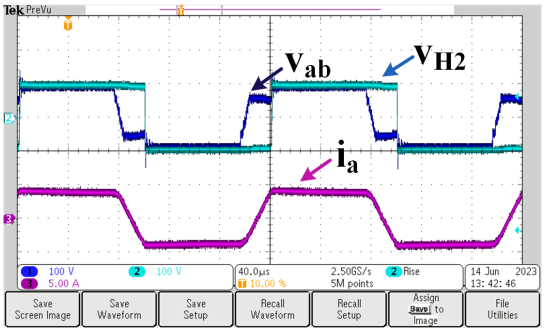

(a)

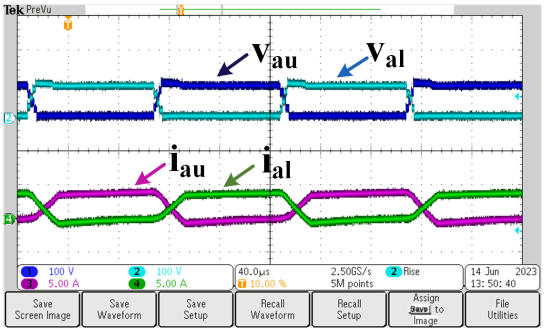

(b)

Fig. 19: Experimental results (a) AC side voltage and current of MMC, and AC side voltage of H-bridge, (b) Arm voltages and currents

depicted in Fig. 19(a), which can obtained based on the voltages and parameters of the system.

The arm voltages and currents of MMC are shown in Fig. 19(b). The MMC generates a Q2L waveform voltage at its arms, and the arm current , which is shown in Fig .19(b), is the summation of half of the DC side current and half of the AC side current. This arm current is compared with the current that is derived by analysis in Fig. 20. As is seen, the analysis results are very close to the experimental results.

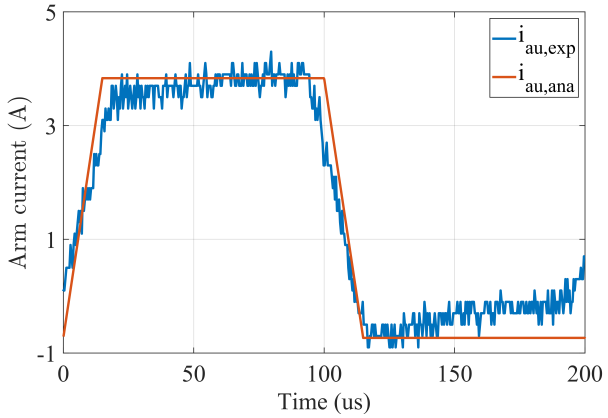

Fig. 20: Upper arm current in experiment and analysis

V. Conclusion

This paper provides an analysis to obtain losses of MMC used in the DAB converter for MVDC grids. In this application, MMC generates an output voltage with Q2L waveform, and H-bridge converter creates a 2-level waveform. In this case, the AC side voltages of MMC and H-bridge converter are approximated, and then, based on the this approximation, the AC side current is determined, which can be used to obtain arm current of MMC. After that, the conduction and switching losses are derived by using the arm current and arm voltage. Finally, the comparison between simulation and experimental results, and the provided analysis shows that the the accuracy of the analysis to determine the total losses is more than 95%.

References

[1] A. Poorfakhraei, M. Narimani and A. Emadi, "A Review of Multilevel Inverter Topologies in Electric Vehicles: Current Status and Future Trends," IEEE Open J. Power Electron., vol. 2, pp. 155-170, March 2021.

[2] N. Meghana, M. Pushparaju, M. Kavitha, N. S. Kalyan Chakravarthy and D. M. Reddy, "A Critical Review on Electric Vehicle Battery Failures and Causes," 2022 IEEE 2nd International Conference on Sustainable Energy and Future Electric Transportation (SeFeT), pp. 1-5, Oct. 2022.

[3] S. Habib, M. M. Khan, F. Abbas, and H. Tang, "Assessment of electric vehicles concerning impacts, charging infrastructure with unidirectional and bidirectional chargers, and power flow comparisons," Int. J. Energy Res., vol. 42, no. 11, pp. 3416–3441, Apr. 2018.

[4] M. R. Khalid, I. A. Khan, S. Hameed, M. S. J. Asghar and J. -S. Ro, "A Comprehensive Review on Structural Topologies, Power Levels, Energy Storage Systems, and Standards for Electric Vehicle Charging Stations and Their Impacts on Grid," in IEEE Access, vol. 9, pp. 128069-128094, Sept. 2021.

[5] L. Camurca, T. Pereira, F. Hoffmann and M. Liserre, "Analysis, Limitations, and Opportunities of Modular Multilevel Converter-Based Architectures in Fast Charging Stations Infrastructures," in IEEE Trans. Power Electron., vol. 37, no. 9, pp. 10747-10760, Sept. 2022.

[6] L. Camurca, X. Gao, L. F. Costa and M. Liserre, "Design of a Medium Voltage DC Fast Charging Station with Grid Voltage Regulation and Central Modular Multilevel Converter," 2018 IEEE Energy Conversion Congress and Exposition (ECCE), pp. 2798-2804, Sept. 2018.

[7] H. Jin, W. Chen, K. Hou, S. Shao, L. Shu, and R. Li, "A sharing-branch modular multilevel DC transformer with wide voltage range regulation for DC distribution grids," IEEE Trans. Power Electron., vol. 37, no. 5, pp. 5714–5730, May 2022.

[8] P. A. Gray, Z. C. Ma and P. W. Lehn, "A High-Frequency MMC for DC–DC Applications Using a Three-Winding Transformer With DC Flux Cancellation," in IEEE J. Emerg. Sel.Topics Ind. Electron., vol. 3, no. 3, pp. 647-657, July 2022.

[9] I. A. Gowaid, G. P. Adam, A. M. Massoud, S. Ahmed, D. Holliday and B. W. Williams, "Quasi Two-Level Operation of Modular Multilevel Converter for Use in a High-Power DC Transformer With DC Fault Isolation Capability," in IEEE Trans. Power Electron., vol. 30, no. 1, pp. 108-123, Jan. 2015.

[10] J. Freytes, F. Gruson, P. Delarue, F. Colas and X. Guillaud, "Losses estimation method by simulation for the modular multilevel converter," 2015 IEEE Electrical Power and Energy Conference (EPEC), pp. 332-338, Oct. 2015.

[11] F. Ertürk and A. M. Hava, "A detailed power loss analysis of modular multilevel converter," emph2015 IEEE Applied Power Electronics Conference and Exposition (APEC), pp. 1658-1665, March 2015.

[12] A. Marquez, J. I. Leon, S. Vazquez, L. G. Franquelo and M. Perez, "A comprehensive comparison of modulation methods for MMC converters," IECON 2017 - 43rd Annual Conference of the IEEE Industrial Electronics Society, pp. 4459-4464, Oct. 2017.

[13] R. Mo, H. Li and Y. Shi, "A Phase-Shifted Square Wave Modulation (PS-SWM) for Modular Multilevel Converter (MMC) and DC Transformer for Medium Voltage Applications," in IEEE Trans. Power Electron., vol. 34, no. 7, pp. 6004-6008, July 2019.

[14] P. F. S. Costa, P. H. B. Löbler, L. Roggia and L. Schuch, "Modeling and Control of DAB Converter Applied to Batteries Charging," in IEEE Trans. Energy Convers., vol. 37, no. 1, pp. 175-184, March 2022.

[15] A. Beddard, C. E. Sheridan, M. Barnes and T. C. Green, "Improved Accuracy Average Value Models of Modular Multilevel Converters," in IEEE Trans. Power Deliv., vol. 31, no. 5, pp. 2260-2269, Oct. 2016.